Linewidths of C2H2 perturbed by H2: experiments and calculations from an ab initio potential

Franck Thibault, Benoît Corretja, Alexandra Viel, Dionisio Bermejo, Raúl Z. Martínez, Béatrice Bussery-Honvault

Linewidths of C_2H_2 perturbed by H_2: experiments and calculations from an *ab initio* potential

Franck Thibault,* Benoît Corretja, and Alexandra Viel

Institut de Physique de Rennes, UMR CNRS 6251,

Université de Rennes I, F-35042 Rennes, France

Dionisio Bermejo and Raúl Z. Martínez

Instituto de Estructura de la Materia, CSIC,

Serrano 123, ES-28006 Madrid, Spain

Béatrice Bussery-Honvault

Institut UTINAM, UMR CNRS 6213,

Université de Franche-Comté,

F-25030 Besançon, France

Abstract

In this work we present a theoretical and experimental study of the acetylene - hydrogen system. A potential surface considering rigid monomers has been obtained by *ab initio* quantum chemistry methods. This 4-dimensional potential is further employed to compute using the close-clouping approach and the coupled-states approximation pressure broadening coefficients of C_2H_2 isotropic Raman Q lines over a temperature range of 77 to 2000 K. Experimental data for the acetylene ν_2 Raman lines broadened by molecular hydrogen are obtained using stimulated Raman spectroscopy. The comparison at 143 K of theoretical values with experimental data is promising. Approximations to increase computational efficiency are proposed.

*E-mail:Franck.Thibault@univ-rennes1.fr

I. INTRODUCTION

The acetylene-hydrogen system is of interest for astrophysical, atmospherical, and combustion applications. It is well known that acetylene is a minor constituent of the hydrogen-dominant atmospheres of Jupiter and Saturn and of the nitrogen-dominant atmosphere, but also containing hydrogen, Saturn's moon Titan. Traces of acetylene are also found in the atmosphere of the giant Uranus and Neptune planets. It has been shown that even if C_2H_2 is present as a trace constituent, it plays an important role in the photochemistry of these atmospheres [refs. 1–6 and references therein]. Acetylene is also a trace constituent of the Earth's atmosphere, mainly produced by anthropogenic sources (see refs in 1–6). From a more applied point of view, acetylene is present in a number of processes of industrial interest: hot-filament-activated C_2H_2–H_2 gas mixtures are used to grow diamond carbon surfaces[7–9] or carbon nanotubes.[10] It is known that acetylene also plays a role as an intermediate species in the process of soot formation often observed in combustion research[11, 12]. Finally, acetylene is frequently used as a target molecule to measure the temperature of combustion mixtures through the use of rotational or vibrational coherent anti-Stokes Raman spectroscopy (CARS) [Ref.13 and references therein]. This application takes advantage of the relative simplicity of C_2H_2 Raman spectrum and the associated large scattering cross section.

To get a better insight into these processes, a detailed knowledge of the collisional broadening of acetylene lines with various gases is desired. A number of studies have been devoted to rare gas-broadening[1–6, 14–17] and some of us have recently presented a series of papers devoted to the acetylene and its interactions with rare gases.[1–5] These weakly bound complexes have received much attention in recent years because their intermolecular potential is mainly affected by the interaction of the rare gas atom with the triple bond of acetylene.[3–5] Works have been dedicated to the calculation of the collisional broadening effects of infrared (IR) or Raman C_2H_2 lines. In the present paper, we extend these studies to the C_2H_2–H_2 system.

Much less attention has been paid to the molecular-broadening of acetylene lines. Experimentally, N_2-, O_2-, H_2-pressure broadening[6, 15–22] and self broadening pressure coefficients[6, 15, 23] have been measured at various temperatures between 147 and 300 K. Before this work, the theoretical studies of molecular partners[18–23] were typically per-

formed on the basis of the Robert-Bonamy semi-classical formalism[24] using semi-empirical potential energy surfaces (PES). Only two of these works dealt with hydrogen.[21, 22] Quantum dynamical studies of collisional line broadening in the case of a linear molecule colliding with another one (eventually the same) are much more laborious than in the case of atomic-molecule systems. The corresponding computer cost is much higher than for semi-classical computations, and thus such quantum calculations are quite rare.[25–30] However they are valuable benchmark calculations to evaluate the accuracy of more approximate methods.

Important information on molecular relaxation phenomena can be obtained from the pressure broadening coefficients for different perturbing gases at different temperatures. This feature has induced numerous experimental and theoretical studies of spectral lineshapes. Pressure broadening is closely linked to state-to-state rate coefficients, especially for isotropic Raman lines. An improved understanding and modeling of planetary atmospheres can be achieved with a better knowledge of H_2 collision-induced lines broadening of acetylene. The pressure broadening data for C_2H_2-H_2 have not yet been analyzed in term of an interaction potential for this system. Since no *ab initio* PES for the title system has been reported, one objective of this study is to build such a surface from first principles.

Over the past decades there has been considerable interest in the weakly-bound complexes of small molecules.[31] Among those, only a small number of studies[32–38] focused on complexes formed by acetylene with various small molecules. Significant progress has been made in the *ab initio* computation of intermolecular interactions. Methods like coupled cluster or symmetry adapted perturbation theory (SAPT) [39–41] together with its more recent extension SAPT(DFT) based on the density functional theory [42] enable the determination of van der Waals intermolecular potentials between closed-shell systems with spectroscopic accuracy. After comparative tests between the available *ab initio* methods, we retain the CCSD(T) method for the determination of the C_2H_2-H_2 PES. While the supermolecular CCSD(T) method has to be corrected for basis set superposition error (BSSE) [43], it is competitive in accuracy with the perturbative and BSSE-free SAPT method (see also Ref. 26 for additional tests).

The accuracy of the surface is tested by a quantum determination of pressure broadening coefficients which are compared with current experimental measurements of isotropic Raman lines of the acetylene ν_2 band at 143 K. The experimental technique used for this purpose is stimulated Raman loss spectroscopy[1, 44]. Such experimental data are the first ones

reported for the title collisional system.

In the next section we briefly describe the experimental setup used in this study. In section III we present the method employed for the *ab initio* determination of the PES. Section IV is devoted to the quantum close-coupling calculations of the collisional dynamics. Results and discussions are given in section V, and finally, concluding remarks and perspectives are summarized in section VI.

II. EXPERIMENT

The spectra recorded and analyzed for this work have been obtained with the stimulated Raman spectrometer of Instituto de Estructura de la Materia in Madrid. The spectrometer has been thoroughly described in a number of previous works [1, 44] and only a brief description of the technique emphasizing the details specific to the present experiment will be given here. In a typical stimulated Raman experiment the sample is simultaneously illuminated with two laser beams while the frequency of one of the beams is scanned. When the frequency difference of the two beams matches the frequency of a Raman transition of the sample under study, a transfer of energy can be observed between the high-frequency beam, which loses intensity, and the low-frequency (Stokes) beam, which gains intensity. Every photon of the high-frequency beam involved in the process produces one photon at the Stokes frequency and one quantum of molecular excitation. Despite the underlying theoretical foundation being relatively complex, stimulated Raman spectra can be seen as the Raman analog of stimulated emission: when the frequency condition is met, the presence of Stokes photons provided by the second laser beam stimulates the generation of more Stokes photons with the same frequency, phase, polarization and directional properties. The process can thus be detected as a net increase in the energy of the Stokes beam and a net loss in the energy of the high-frequency beam. The intensity of either beam can be monitored against the frequency to provide a Raman spectrum of the sample. The main strength of this type of experiment (by comparison with linear Raman spectroscopy) is the fact that the instrumental resolution is not limited by dispersive or interferometric elements used to analyze the scattered radiation, but only by the linewidths of the lasers used.

The Ar^+ laser that generates the probe beam is operated at 529 nm and in a single-mode configuration by means of a temperature-stabilized intra-cavity étalon. The laser frequency

is electronically locked to the transmission fringe of an external Fabry-Perot interferometer, reducing the fast frequency jitter to 500 kHz. The frequency of the transmission fringe is in turn locked to the frequency of a molecular reference ($^{130}Te_2$ for these experiments) by means of a secondary stabilization loop that uses a sub-Doppler polarization setup. In this way, the laser frequency is stabilized against both short and long-term drifts and is also known to high accuracy. It must be noted that the frequencies of the spectral lines measured in the course of this work are well known, but since the present measurements rely on accurate fitting of line profiles, it is important to maintain proper laser stability and to avoid frequency drift that could alter the profiles while they are being recorded. The cw ring dye laser that generates the seed for the tunable pump beam is operated with Rhodamine 590, and this seed is later amplified in a pulsed dye amplifier operated with Kiton Red. The amplifier is pumped by the second harmonic of a pulsed, single-mode Nd:YAG laser. The resulting pump pulses have typical energies of ∼3 mJ and a nearly Gaussian temporal profile of 12 ns FWHM, which translates into a Gaussian spectral profile of ∼70 MHz FWHM.

The two beams are overlapped with a dichroic mirror, focused into the sample cell using an f=500 mm planoconvex lens and then recollimated by a similar lens at the exit. In order to improve the S/N ratio of the experiment, two additional broadband mirrors are used to arrange a triple pass through the cell. After the triple pass the laser beams are separated and the probe beam is taken to a fast PIN silicon photodiode. The Raman loss signals thus detected are then amplified and processed by a boxcar integrator. The output of this integrator is sent to a computer where the representation of the Raman loss signal versus the frequency scan of the ring dye laser provides the high resolution Raman spectrum of the sample.

The sample cell is a variation of a design already in use in our laboratory for low-temperature measurements.[1] The system is based on the controlled evaporation of liquid nitrogen to generate a continuous flow of cold nitrogen vapor that is circulated through one of the jackets of the sample cell and cools down the sample. The final temperature can be adjusted by controlling the rate of evaporation. The cell is a tubular pyrex design of approximately 95 cm in length and 10 cm outer diameter, and consists of three internal concentric chambers also tubular in shape and totally isolated from each other. The innermost chamber is the sample chamber, and brewster angle fused silica windows have been installed on both ends so that the laser beams can travel through the cell. The middle chamber is

the one through which the cold nitrogen vapor flows. Finally, the outer chamber is used as isolation chamber to prevent heating of the two inner chambers by the lab atmosphere. To this end, the chamber is pumped to a moderately high vacuum ($\sim 10^{-5}$ torr) and its outer wall lined with mylar foil. Each one of the chambers has its own gas inlet/outlet and valve. For the middle chamber, special consideration had to be paid to the possibility of temperature gradients forming along the cell, since the cold nitrogen vapor warms up as it travels through it. To minimize this effect the nitrogen enters the chamber through a central inlet and exits through two outlets symmetrically located near both ends of the cell. A thermocouple installed in the inner chamber is used to measure the sample temperature at the center of this chamber, where the largest contribution to the Raman signal is generated.

The nitrogen evaporation system consists of a 50-liter dewar in which a ceramic resistor has been submerged. The power dissipated by the resistor, and thus the amount of nitrogen evaporated by unit of time, is controlled with a variac. The vapor generated is conducted, through thermally isolated tubing, to the inlet in the sample cell. In this way, changes in the sample temperature can be accurately induced/controlled by changing the variac voltage. With this system, sample temperatures as low as $\sim$120 K have been reached in our laboratory. The present experiments are conducted at a temperature of 143 K, slightly above the point of deposition of $^{12}C_2H_2$ for the highest of the partial pressures used.

The samples for the experiments consist of diluted mixtures of $^{12}C_2H_2$ (5% in volume) in H_2 at different pressures (20, 40, 60, 80 and 100 mb approximately). All the samples are prepared at least 24 hours in advance in order to ensure proper mixture of the two gases.

Raman spectra of the Q-branch of the ν_2 band of $^{12}C_2H_2$ are recorded up to $j = 17$ for all pressures. Beyond this line, the S/N ratio at the lowest pressures is too poor at this temperature to obtain accurate linewidth data. The spectral lines are analyzed by fitting them to Voigt profiles, either individually or simultaneously when partial overlapping of the lines makes it necessary, as it is the case with the first lines of the band. The Gaussian part of the Voigt profile results from the convolution of the Gaussian Doppler width at 143 K and the Gaussian apparatus function. This part of the Voigt profile can thus be pre-calculated and kept fixed during the fit of the profiles. In this way the Lorentzian contribution to the Voigt profile of each spectral line could be extracted.

To obtain the pressure broadening coefficients, a linear fit of Lorentzian width versus pressure is carried out for each spectral line. The slope of the fit provides the pressure

broadening coefficient of that line.

III. A C_2H_2-H_2 INTERMOLECULAR POTENTIAL

A. *Ab initio* calculations

Different methods are available to treat van der Waals interaction potentials between dimers with an accuracy close to one wavenumber. In order to reach such an accuracy, we have tested different methods and basis sets to evaluate the interaction potential of C_2H_2-H_2. Convergence with respect to the size of the basis set has thus been tested. With van der Waals interactions, binding energies are small and thus, relative variation among them can be large. To perform the calculations, we have used the Molpro package[45] which permits the use of *ab initio* methods such as: the Hartree-Fock (HF) method, the second order Møller-Plesset perturbation theory (MP2), the coupled cluster method at a level of single and double excitations with the triple excitations included perturbatively, i.e. CCSD(T), and the symmetry adapted perturbation method based on monomer orbitals built up with the density functional theory (SAPT(DFT)) [42]. Several atomic basis sets have been tested: the augmented - correlation consistent - polarized triple and quadruple zeta basis sets (aug-cc-pVXZ with X=T and Q) and the polarization optimized Sadlej basis set [46]. We add to this Sadlej set a polarization orbital "d" for the H atoms taken from the aug-cc-pVTZ basis set to obtain [3s2p1d] contracted Gaussian functions for H atoms and [5s3p2d] for C atoms. In all cases, mid-bond functions as proposed by Tao and Pan[47] have been included to improve the convergence of the calculation of the dispersion energy without increasing too much the number of basis functions of the whole system. This adds (3s3p2d1f) functions (with exponents s,p: 0.90, 0.30, 0.10 ; d: 0.60, 0.20 ; f: 0.30) in the basis set.

To test the influence of the choice of the *ab initio* method and of the basis set, we have conducted potential energy calculations for specific conformations (R, θ_A, θ_B, ϕ) of the C_2H_2-H_2 dimer where (R, θ_A, θ_B, ϕ) are the four angular Jacobi coordinates which describe the relative orientation of the two monomers. R is the distance between the two monomer centers of mass and defines the intermolecular axis, $\theta_{\{A,B\}}$ defines the bending angle of the monomer axis relative to the intermolecular axis (the "A" index refers to C_2H_2 while "B" refers to H_2) and ϕ is the rotational angle around R of one monomer relative to the other.

So, specific conformations can be defined as (θ_A, θ_B, ϕ) =(90, 90, 90) (noted X), (0, 0, 0) (L), (90, 90, 0) (H) , (90, 0, 0) (T_a) and (0, 90, 0) (T_b) (see pictorial representations in fig 1 of Ref 48).

All the above selected methods are not equivalent to treat van der Waals interactions as some, like CCSD(T), are supermolecular while others, like SAPT(DFT), are based on a perturbative treatment. So, the former ones will give values incorporating basis set superposition errors (BSSE) while the later ones will be free of BSSE.[49] This error is a consequence of the unphysical lowering of the monomer energies due to the presence of the basis functions at the other site. In order to compare both methods, we have used the Boys and Bernardi approach[43] to correct the CCSD(T) energies for BSSE. This approach, also called counterpoise (CP) recipe, suggests to compute the interaction energy as the difference of the "supermolecule" AB energy with the monomer energies calculated in the full dimer basis.[49] For that, we define $E_X(Y)$ as the energy of the system X in the basis set Y. The BSSE-free interaction energy is obtained as $E_{AB}^{CP} = E_{AB}(AB) - E_A(AB) - E_B(AB)$ while the BSSE correction is evaluated by: $E_A(A) + E_B(B) - E_A(AB) - E_B(AB)$. In view of all these tests, we concluded that the energies evaluated with the CCSD(T) method and the Sadlej basis set give converged energies with a sufficient accuracy keeping a good ratio of computer time required relative to the accuracy. As may be seen in Fig. 1, the results at the CCSD(T) level compare well to the SAPT(DFT) levels for three geometries.

For the *ab initio* determination of the interaction potential, both monomers are treated as rigid and fixed at their vibrationally ground equilibrium geometry, i.e. $r_{CC} = 2.283$ bohr for C-C bond and $r_{CH} = 1.999$ bohr for C-H bond of C_2H_2, $r_{HH} = 1.449$ bohr for the H-H bond of H_2. Computations are performed for a large number of geometries located on a (R, θ_A, θ_B, ϕ) grid. The product grid includes 20 values of R (bohr) = [5.00, 5.50, 6.00, 6.25, 6.50, 6.75, 7.00, 7.25, 7.50, 7.75, 8.00, 8.25, 8.50, 8.75, 9.00, 9.50, 10.00, 12.00, 15.00, 20.00], 9 values of θ_A and θ_B (degree)= [0.00, 11.25, 22.50, 33.75, 45.00, 56.25, 67.50, 78.75, 90.00], 17 values of ϕ (degree)= [0.00, 11.25, 22.50, 33.75, 45.00, 56.25, 67.50, 78.75, 90.00, 101.25, 112.50, 123.75, 135.00, 146.25, 157.50, 168.75, 180] and results in 27540 geometries. An electronic file containing the *ab initio* energies is available upon request to the authors.

The current study is performed within a reduced dimensionality approach in which the two molecules are rigid linear rotors. The range of the error corresponding to the rigid treatment can be estimated from a static study including geometrical modifications of C_2H_2.

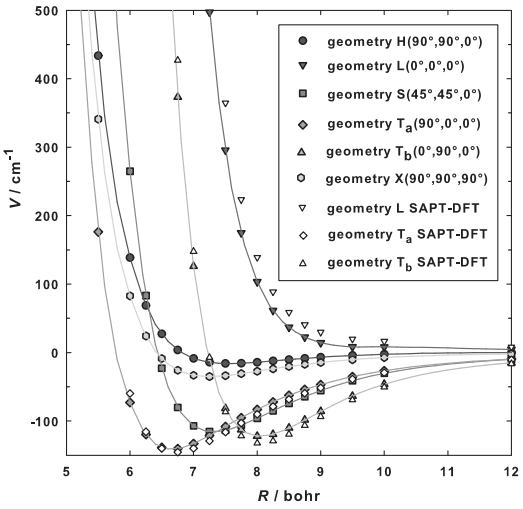

FIG. 1: Selected angular cuts of the PES as a function of the intermolecular distance R. Symbols represent the *ab initio* values. CCSD(T) *ab initio* energies are compared with SAPT(DFT) values for three angular approaches.

The lowest frequency mode of C_2H_2 being for the bending motions, a study of the energy change when a CH bond of C_2H_2 is bent has been investigated. The results show that conformations which take this bending modification into account are more stable only at very short intermolecular distance (<5.5 bohr). The energy difference with or without C-H bending is negligible ($\sim$ 2 cm^{-1} for the H geometry near 5 bohr). Therefore, we conclude that treating C_2H_2 as a rigid rotor is a good approximation for the temperature regime of interest.

B. Representation of the potential energy surface

In order to perform the quantum dynamical study of the collision, an amenable form of the C_2H_2-H_2 interaction potential is necessary. A development onto bispherical harmonics[26, 50, 51] has been used. This expansion,

$$V\left(R,\theta_A,\theta_B,\phi\right)=\sum_{L_A,L_B,L}V_{L_A,L_B,L}\left(R\right)A_{L_A,L_B,L}\left(\theta_A,\theta_B,\phi\right) \tag{1}$$

is restricted to even L_A, L_B and L because the colliding partners are homonuclear molecules. As usual, the relation $|L_A-L_B|\leq L\leq|L_A+L_B|$ has to be fulfilled in eq. (1). In the case of two linear molecules, the angular functions $A_{L_A,L_B,L}\left(\theta_A,\theta_B,\phi\right)$ are defined by normalized products of spherical harmonics for monomers A and B,

$$A_{L_A,L_B,L}\left(\theta_A,\theta_B,\phi=\phi_A-\phi_B\right)=\left(\frac{2L+1}{4\pi}\right)^{1/2}\sum_m\langle L_AmL_Bm|L0\rangle Y_{L_A}^m\left(\theta_A,\phi_A\right)Y_{L_B}^{-m}\left(\theta_B,\phi_B\right) \tag{2}$$

where $Y_{L_A}^m$ and $Y_{L_B}^{-m}$ are spherical harmonics, $\langle\cdots|\cdots\rangle$ Clebsch-Gordan coefficients, and $|m|\leq\min\left(L_A,L_B\right)$. The development in eq. (1) has been limited to 30 angular functions as described in the work of A. van der Avoird *et al* on the N_2-N_2 PES (see the first column of table II of ref. [51]). This development allows the *ab initio* points to be represented to better than 2% at long range and better than 8% at shorter intermolecular distances. A further restriction to only 23 terms (thus removing all the terms with $L_B=6$ and the $V_{6,4,10}$ term), does not affect the value of the pressure broadening (PB) cross sections, even if the *ab initio* points are less well reproduced. The radial coefficients, $V_{L_A,L_B,L}\left(R\right)$, for the tabulated R values, are obtained using Gauss-Legendre quadratures over θ_A and θ_B, and a Chebyshev quadrature over ϕ [26, 52]. A standard interpolation method [52] is then used to compute the radial coefficients for R values needed in the dynamical treatment.

This representation of the PES has the expansion most compatible for efficient use with the MOLSCAT code[53], thus saving CPU time.

IV. CALCULATIONS OF PRESSURE BROADENING CROSS SECTIONS

Pressure broadening, thus the modification of the spectral lineshapes of a molecule induced by the presence of nearby particles, is sensitive to the molecular interaction. Comparison of computed and measured PB coefficients is thus a test of the validity of the interaction

potential we propose. The method of calculations is very similar to that used for our N_2-H_2 study[26] and thus only the salient details will be given here.

The collisional broadening cross-sections, using the impact approximation [54, 55], can be expressed as a function of binary diffusion S-matrix elements [25, 56] obtained from the MOLSCAT quantum dynamical code. To solve the coupled equations with MOLSCAT code, the propagation is carried out with the diabatic modified log-derivative method from a minimum distance of 4.5 bohr to an intermediate one of 17 bohr and with the Airy method up to a maximum intermolecular distance $R = 21$ bohr. Convergence in the cross sections is typically reached for total angular momentum J ($\vec{J} = \vec{j}_{AB} + \vec{\ell}$, in which j_{AB} is the composed angular momentum formed by the two molecules and ℓ is associated with the relative motion of the colliding pair) varying approximately from 45 to 60 for kinetic energies between 150 cm^{-1} and 700 cm^{-1}.

All energetically open rotational levels (j_A, j_B) and the asymptotically closed levels lying within approximately 100 cm^{-1} above the total energy are included in the rotational basis to perform the scattering calculations for each total energy. The total energy is defined within the rigid rotor approximation by $E_T = E_{kin} + B_A j_A (j_A + 1) + B_B j_B (j_B + 1)$ with $B_A = 1.1766$ cm^{-1} (for C_2H_2) and $B_B = 60.$ cm^{-1} (for H_2).

It is assumed that both acetylene and hydrogen molecules are composed of two noninterconverting species in our experiment. Natural nH_2 is a 3:1 mixture of ortho and para hydrogen (oH_2 and pH_2) species with odd and even j_2, respectively. Acetylene is also a mixture of ortho and para species.

Since, in the rigid rotor approximation, the PB cross section of an isotropic Raman line is simply the sum of two-body rotational state to state cross sections[27], we have performed four types of calculations of state-to-state cross sections: calculations for ortho-ortho, para-ortho, ortho-para and para-para species. For each of these pairs, we performed more than 190 computations for total energies E_T between 7 and 1600 cm^{-1} using the close coupling scheme and 4 additional calculations at 2000, 2500, 3000 and 4000 cm^{-1} using the coupled states method (for a review of these quantum dynamical methods see for instance Ref 57), all using the MOLSCAT package.

Defining[26, 27] a partial pressure broadening cross section as

$$\sigma (j_A, j_B, E_{kin}) = \sum_{j'_A, j'_B} \sigma \left(j_A j_B \rightarrow j'_A j'_B; E_{kin} \right) \tag{3}$$

with $j_A^{'} \neq j_A$, and using the Maxwell Boltzmann thermal average based on the kinetic energies,

$$\sigma(j_A, j_B, T) = \frac{1}{(k_B T)^2} \int \sigma(j_A, j_B, E_{kin}) E_{kin} \exp\left(-E_{kin}/k_B T\right) dE_{kin}, \tag{4}$$

the PB cross section at temperature T of a $Q(j_A)$ line is a sum of 2 contributions:

$$\sigma\left(j_A, T\right) = \frac{1}{4}\sigma_{\mathrm{pH_2}}\left(j_A, T\right) + \frac{3}{4}\sigma_{\mathrm{oH_2}}\left(j_A, T\right) \tag{5a}$$

with

$$\sigma_{\mathrm{pH_2}}\left(j_A, T\right) = \sum_{j_B \text{ even}} \rho_{j_B} \sigma\left(j_A, j_B, T\right) \tag{5b}$$

and

$$\sigma_{\mathrm{oH_2}}\left(j_A, T\right) = \sum_{j_B \text{ odd}} \rho_{j_B} \sigma\left(j_A, j_B, T\right). \tag{5c}$$

Finally, the PB coefficient (in cm^{-1}) is given by [56]

$$\gamma\left(j_A\right) = \frac{n_{H_2} \bar{v}}{2\pi c} \sigma\left(j_A, T\right). \tag{6}$$

This quantity can be compared with the measurements of experiments performed at a given temperature T with $\mathrm{nH_2}$ and $\mathrm{nC_2H_2}$. In eqs. (5), ρ_{j_B} is the $\mathrm{H_2}$ (unit) normalized rotational populations for each $\mathrm{H_2}$ species, n_{H_2} the density of hydrogen and $\bar{v}$ is the mean relative speed $\bar{v} = \sqrt{\frac{8 k_B T}{\pi \mu}}$, with $\mu = 1.865$ u being the reduced mass of the colliding pair.

The computation of pressure broadening coefficients of infrared R and P lines relies on a more elaborate theory and requires more computational power[25, 54–56] since both even and odd angular momenta of $\mathrm{C_2H_2}$ need to be included at the same time. The PB coefficients may be expressed as[58–60]

$$\gamma\left(j, j^{'}\right) = \frac{1}{2}\left(\gamma(j) + \gamma(j^{'})\right) + \gamma_{\mathrm{elastic}} \tag{7}$$

with $j^{'} = j \pm 1$. The first term contains the inelastic contributions and the last term is due to elastic effects. Within the "random phase approximation"(RPA)[58] in which the elastic contribution is neglected, the PB coefficient of such a line is given as the half sum of two isotropic Raman Q-lines.

V. RESULTS AND DISCUSSIONS

A. *Ab initio* PES calculation

Fig. 1 displays angular cuts of the CCSD(T) PES for various geometries. The linear geometry is purely repulsive while the T_a geometry is the most attractive. The repulsive part of the L geometry approach occurs at quite large intermolecular distances due to the long size of C_2H_2 given the definition of R from center of masses. The strong core-core repulsion is thus seen at larger R values than for the other geometries. For similar reason, the core-core repulsion is seen at lower R distance in the T_a approach where H_2 is pointing towards C_2H_2 than in the T_b one where C_2H_2 is pointing towards H_2. The attractive part of the PES is found to be due to the quadrupole-quadrupole interaction both in the T_a and T_b geometries. In the L approach, the quadrupole-quadrupole interaction is repulsive. The global minimum value of -141 cm^{-1} is found at an intermolecular distance of 6.7 bohr. The T_b geometry has a minimum of about -122 cm^{-1} located at $R = 8$ bohr and the H geometry is only very slightly attractive around 7.6 bohr. Therefore this PES is quite anisotropic in the well region and in its repulsive part. This last point is easily understandable bearing in mind that this repulsive part is very sensitive to the steric effect induced by the "long" linear acetylene molecule.

The anisotropy of the PES can be also seen on Fig. 2 which presents a selection of radial coefficients $V_{L_A,L_B,L}$ of the potential development. The most relevant components are the V_{202} which represents[48] the interaction of the acetylene quadrupole with the spherical part of the H_2 molecule, the V_{224} which resumes to the quadrupole - quadrupole interaction at large distances, the V_{426} (hexadecapole-quadrupole) and the V_{022} (spherical part of the acetylene with the quadrupole moment of hydrogen). The contribution of the other terms is significant only at short distances where the anisotropy is high.

The only *ab initio* study on the C_2H_2-H_2 system has been done by Sapse et al.[38] for which a single geometry configuration has been computed, thus limiting the comparison with our work. Yang and Watts[37] determined an empirical PES but considering the H_2 molecule as a spherical partner using measured total differential cross sections. Nonetheless, we can compare the C_2H_2-H_2 PES with the N_2-H_2 one.[26, 61] The C_2H_2-H_2 potential is deeper and more anisotropic than the N_2-H_2 potential. We infer that this is due to

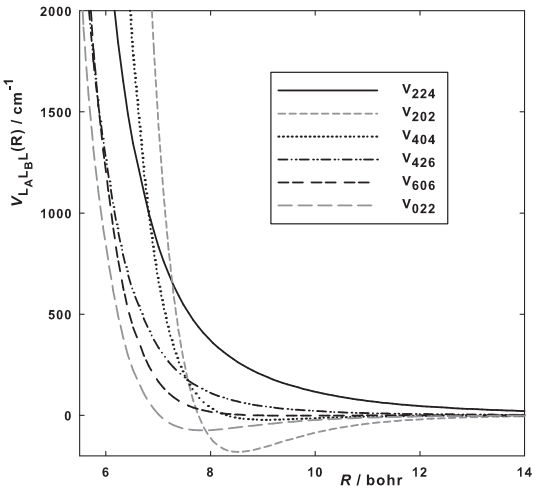

FIG. 2: Main anisotropic components of the PES (see eq. (1)).

the fact that the magnitude of the quadrupole moment of the acetylene is roughly 4.5 times[62, 63] the quadrupole of N_2,[61] and that the polarizability as well as the anisotropic polarizability of the acetylene are larger for acetylene (roughly twice) than for nitrogen.[61, 63] The anisotropy at short range is greater for C_2H_2-H_2 because the acetylene molecule is longer than the nitrogen molecule. Moreover, we observe stronger binding energies for C_2H_2-H_2 relatively to C_2H_2-He[64] resulting from the stronger (4 times) H_2 polarizability relatively to the He's one, and from a more favorable electron exchange of C_2H_2 with H_2 due to the diatomic character of H_2.

B. Pressure broadening cross sections and coefficients

Because quantum studies of pressure broadening cross sections for linear - linear molecules are quite scarce[26–30] we will first discuss the present theoretical results. Fig. 3 gives details

of a selection of partial PB cross sections. It provides the contribution, defined by eq. (3),

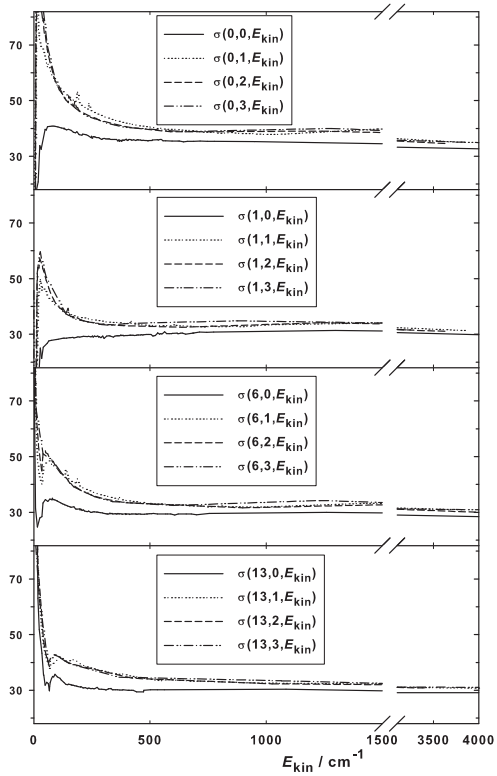

FIG. 3: Selected partial pressure broadening cross section $\sigma\left(j_A, j_B; E_{kin}\right)$ [in Å^2] as a function of the relative kinetic energy [in cm^{-1}].

from various rotational quantum number of H_2 ($j_B = 0, 1, 2, 3$) to the PB cross sections (eq. (5)) for $j_A = 0, 1, 6, 13$. The cross sections for populated larger j_B (4 and 5) are not shown for clarity reasons but they are very close to the ones with $j_B = 2$ or 3, especially for kinetic energies greater than about 500 cm^{-1}. On this basis, the calculations may be simplified and CPU time reduced.

In examining Fig. 3, it is to be noted that all the coupling terms $V_{0,L_B,L}$ of the potential do not enter in the partial PB cross section (eqn.(3)) because such terms induce a rotationally elastic transition for the optically active molecule (see eq.(9) of Ref. 50). In addition, based on the SAPT(DFT) study which provides the different contributions (electrostatic, dispersion, exchange, ...) to the potential, we can assert that the electrostatic interactions dominate only at intermolecular distances larger than about 9 bohr.

The PB cross sections $\sigma\left(j_A, 0; E_{kin}\right)$ are the smallest regardless of the value of j_A because the coupling via the permanent multipolar (essentially quadrupole) moments of the H_2 molecule vanishes and the anisotropy which induces inelastic transitions is the smallest. In other words, in the entrance collisional channel the H_2 molecule is effectively spherical and the V_{224} term has a small influence because it implies a post-collisional value $j_B^{'} = 2$ with a weak probability transition, especially at low kinetic energy. On the contrary, for $j_B > 0$, the selection rules on the final $j_B^{'}$ value allow for inelastic as well as elastic transitions for the H_2 molecule. Therefore the cross sections for $j_B > 0$ are larger than the $j_B = 0$ ones. At high energy (> 2000 cm^{-1}) the cross sections with $j_B = 0$ become similar to the ones with $j_B > 0$ because collisions are sensitive primarily to the repulsive part of the PES where the V_{224} no longer dominates over the other terms (see Fig. 2) which induce more transitions. In the low or very low kinetic energy regime, which essentially probes the long range part of the potential, we note the very quick decrease of the partial PB cross sections for $j_A = 0$ and 1 (especially for $j_B = 0$). In these levels, the acetylene molecule cannot relax. Moreover, the PB cross sections for $j_A = 1$ is smaller than for $j_A = 0$. This may have two reasons. First, this may be due to a steric effect, indeed the apparent cross section is smaller in $j_A = 1$ than in $j_A = 0$ because in the former the acetylene molecule has preferential orientations. Second, the energy required to make an upward transition starting from $j_A = 1$ to $j_A^{'} = 3$ is nearly twice that required for $j_A = 0$ to $j_A^{'} = 2$. Finally, we observe that these partial cross sections for low j_A are larger than cross sections for high j_A values. This behavior is the same as observed for atomic perturbers. [1–5]

We also observe that these quantities have slow and smooth variations with increasing kinetic energy, therefore the calculation of the thermal average is no longer necessary for high temperatures. The thermally averaged cross section in eq. (6) can thus be replaced with the value obtained at the single kinetic energy $\bar{E}_{kin} = \frac{4}{\pi} k_B T/hc$ associated to the mean speed at the temperature T:

$$\sigma\left(j_A, T\right) = \sigma(j_A, \bar{E}_{kin}). \tag{8}$$

Table I provides thermally averaged (partial) PB cross sections of C_2H_2 perturbed by H_2 for $T = 295$ and 1500 K. We confirm that the PB cross sections for $j_B = 0$ are the smallest, but more importantly we note that the cross sections for $j_B = 1, 2, 3$ are very close to each other. Thus it is not crucial, especially at high temperatures where the duration of the calculations drastically increases, to compute such quantities for $j_B > 3$. We have verified

TABLE I: Selected thermally averaged partial PB cross sections at 295 and 1500 K (see eqs. (3) and (4))

	T=295 K				T=1500 K			
j_A	$j_B=0$	$j_B=1$	$j_B=2$	$j_B=3$	$j_B=0$	$j_B=1$	$j_B=2$	$j_B=3$
0	36.58	45.53	45.03	45.04	32.99	36.99	36.58	37.60
1	29.32	35.24	35.43	35.41	29.36	31.95	31.61	32.43
2	29.10	35.58	35.32	35.17	28.63	31.65	32.78	32.27
3	29.33	35.68	35.16	35.81	28.42	31.25	30.82	31.85
4	29.78	36.27	36.17	35.89	28.89	31.26	33.29	31.92
5	30.24	36.48	36.12	36.73	28.30	31.28	30.82	31.76
6	30.42	36.91	36.86	36.47	29.03	31.38	33.50	32.17
7	30.82	36.98	36.64	36.56	28.42	31.42	30.99	31.83
8	30.74	37.23	37.13	36.77	29.14	31.47	33.34	32.01
9	31.10	37.25	36.90	36.81	28.56	31.42	31.05	31.61
10	31.02	37.31	37.14	36.72	29.24	31.44	33.42	31.67
11	31.38	37.31	36.99	36.63	28.74	31.36	31.20	31.14
12	31.14	37.20	36.88	36.17	29.46	31.36	33.68	31.32
13	31.61	37.13	36.75	35.95	28.77	31.23	31.15	30.84
14	31.44	36.90	36.60	35.25	29.51	31.13	33.69	31.00
15	31.74	36.65	37.48	35.19	28.73	31.05	31.01	30.37

this using j_B values up to 5. To economize CPU time one can replace $\sigma(j_A, j_B > 3; T)$ in eq. (5b) or (5c) by a mean value deduced from the first j_B values. At 295 K roughly half of the pH_2 molecules are in $j_B = 0$ and that this population quickly decreases as the temperature increases. Moreover (Fig. 3 and Table I) the partial PB cross sections become identical to each other as T increases.

Using the data given in Table I, it can be easily shown that at room temperature the para cross section defined in eq. (5b) is about 9% lower than the ortho cross section eq. (5c) for all j_A values while at 1500 K the difference is only about 3%. Thus at high temperature it is not essential to compute the pH_2 cross sections. Instead it may be assumed that

$\sigma_{pH_2} = \sigma_{oH_2}$. Such a behavior is also observed[65] for N_2-N_2 but at lower temperatures because the rotational constant for N_2 is much smaller than the one for H_2 and thus the number of populated states increases quickly with the energy.

The grid used for the kinetic energies allows the evaluation of the PB coefficients at various temperatures between 77 and 2000 K. This is of interest for future use in studies related to planetology, circumstellar envelope or combustion. The PB coefficients at any temperature can be retrieved using the following semi-empirical relation,

$$\gamma_j(T) = \gamma_j(T_0) \left(\frac{T_0}{T}\right)^{n_j}, \tag{9}$$

where the reference temperature T_0 has been chosen at 295 K. Because such a relation cannot provide[66, 67] the temperature dependence of the half width at half maximum (HWHM) over all this range of temperature, table II gives the n-exponent for $T < 295$ K and $T > 295$ K. Note that n is smaller for the higher temperatures and tends to the classical limit of 0.5 (hard sphere partners).

C. Comparison with experimental data

The results of our calculations are now compared with experimental results. Experimental PB coefficients of isotropic Raman lines, at 143 K, are tabulated in Table III and compared with calculations in Fig. 4. Taking into account the experimental error bars, a good agreement between the current experimental data and our calculations is observed. Moreover, there is no substantial disagreement even using eq. (6) without performing the thermal average over the relative kinetic energies (eq. (8)). For instance for the $Q(1)$ line the relative difference between the proper thermally averaged value and the non averaged value is only about 4%.

We can also compare our theoretical results for isotropic Raman lines with measurements performed in IR bands.[6, 21, 22] Figs. 5 and 6 compare such data at 173 and 295 K. The results of their comparison are very similar to what is observed for atom - linear molecule.[59, 60, 66] Pressure broadening coefficients for low j values which are sensitive to interactions in both the short and long range parts of the PES and to elastic effects (for IR lines) are very different for R and Q lines. For "high" j, the PB coefficients for R and Q lines are similar because they are primarily sensitive to the repulsive part of the PES which induces

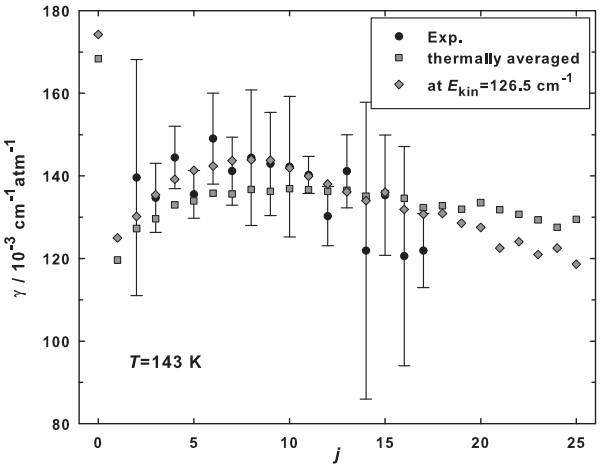

FIG. 4: Comparison between experimental and calculated PB coefficients of isotropic Raman lines. Displayed theoretical values are the ones obtained through the thermal average of the PB cross section and the ones at the single kinetic energy $\frac{4}{\pi}k_BT/hc$ associated to the mean speed at 143 K.

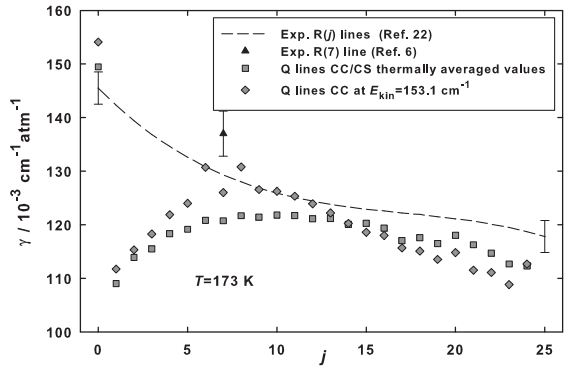

FIG. 5: Comparison between experimental[6, 22] pressure broadening coefficients of R lines and calculated (same as Fig. 4) values for Q lines at 173 K.

essentially inelastic collisions.[59, 60, 66, 68, 69] We also note that the RPA (see eq. (7)) would only improve the agreement for the very lowest j values but would not significantly change other values (not shown). As expected,[2–5, 26, 59, 60, 66] the agreement between thermally averaged values and non averaged values improves as the kinetic energies (and thus the temperature) increase. Finally, we observe that quite good agreement is obtained with the experimental values for j greater than about 10, especially at room temperature.

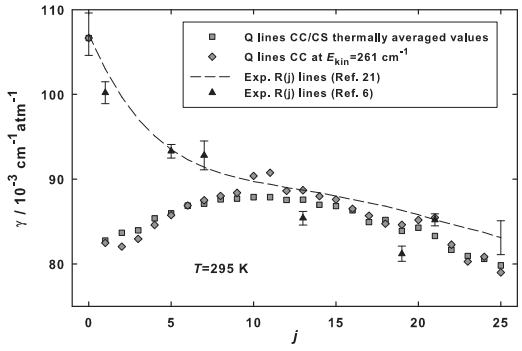

FIG. 6: Comparison between experimental[6, 21] pressure broadening coefficients of R lines and calculated (same as Fig. 4) values for Q lines at 295 K.

VI. CONCLUSION

We have determined an acetylene - hydrogen PES at the CCSD(T) level on a four dimensional grid with the monomers taken as rigid rotors. Using this potential, we have calculated pressure broadening cross sections on a wide range of energies allowing the determination of pressure broadening coefficients up to 2000 K. Because close coupling calculations are quite time consuming, we discerned means of improving computational efficiency. Results of our calculations are in good agreement with experimental pressure broadening coefficients of the acetylene ν_2 Raman lines measured in a bath of H_2 at 143 K. Additional comparisons of theoretical Raman Q linewidths with pressure broadening coefficients of IR acetylene lines measured at 173 and 295 K are also encouraging. The computation of the IR pressure line-broadening coefficients is currently in progress in the group and will be compared to available experimental data.

Acknowledgments

The authors thank Margot Mandy, University of Northern British Columbia, Canada, for her careful reading of this manuscript.

TABLE II: Temperature dependence of the PB coefficients (see eq.(9))

j	γ_j(295 K)	n T<295 K	n T>295 K
0	106.66	0.63	0.56
1	82.74	0.51	0.51
2	83.67	0.58	0.51
3	83.97	0.60	0.54
4	85.37	0.61	0.54
5	85.96	0.61	0.56
6	86.87	0.62	0.55
7	87.11	0.61	0.57
8	87.61	0.61	0.55
9	87.69	0.61	0.57
10	87.89	0.61	0.55
11	87.88	0.61	0.58
12	87.55	0.61	0.55
13	87.57	0.61	0.57
14	86.98	0.61	0.54
15	86.83	0.61	0.56
16	86.33	0.61	0.54
17	84.93	0.61	0.55
18	85.17	0.61	0.55
19	83.90	0.62	0.55
20	84.28	0.63	0.54
21	83.29	0.63	0.54
22	81.67	0.63	0.55
23	80.93	0.65	0.54
24	80.61	0.61	0.53

TABLE III: Comparison between measured and calculated pressure broadening coefficients, in 10^{-3}cm^{-1}/Atm, of isotropic Raman lines at 143 K.

j	theory	exp
0	174.25	
1	125.0	
2	130.2	139.6 ± 28
3	135.4	134.7 ± 8.
4	139.15	144.4 ± 8.
5	141.30	135.5 ± 6
6	142.35	149. ± 11
7	143.7	141.1 ± 8
8	143.9	144.4 ± 16
9	143.8	142.9 ± 12
10	141.9	142.2 ± 17
11	139.9	140.2 ± 4
12	138.05	130.2 ± 7
13	136.15	141.1 ± 9
14	134.0	121.9 ± 36
15	136.05	135.3 ± 15
16	131.85	120.6 ± 27
17	130.7	121.9 ± 9
18	130.9	
19	128.55	
20	127.55	
21	122.55	
22	124.05	
23	120.95	
24	122.50	
25	118.6	

[1] J. L. Domenech, F. Thibault, D. Bermejo, and J.-P. Bouanich, *J. Mol. Spectrosc.*, 2004, **225**, 48–54.

[2] F. Thibault, *J. Mol. Spectrosc.*, 2005, **234**, 287–289.

[3] D. Cappelletti, M. Bartolomei, M. Sabido, F. Pirani, G. Blanquet, J. Walrand, J.-P. Bouanich, and F. Thibault, *J. Phys. Chem. A*, 2005, **109**, 8471–8480.

[4] D. Cappelletti, M. Bartolomei, E. Carmona-Novillo, F. Pirani, G. Blanquet, and F. Thibault, *J. Chem. Phys.*, 2007, **126**, 064311.1–11.

[5] F. Thibault, D. Cappelletti, F. Pirani, G. Blanquet, and M. Bartolomei, *Eur. Phys. J. D.*, 2007, **44**, 337–344.

[6] P. Varanasi, *J. Quant. Spectrosc. Radiat. Transfer*, 1992, **47**, 263–274.

[7] M. N. R. Ashfold, P. W. May, J. R. Petherbridge, K. N. Rosser, J. A. Smith, Y. A. Mankelevich, and N. V. Suetin, *Phys. Chem. Chem. Phys.*, 2001, **3**, 3471–3485.

[8] J. A. Smith, E. Cameron, M. N. R. Ashfold, Y. A. Mankelevich, and N. V. Suetin, *Diamond and related Materials*, 2001, **10**, 358–363.

[9] A. Cheesman, J. A. Smith, M. N. R. Ashfold, N. Langfold, S. Wright, and G. Duxbury, *J. Phys. Chem. A*, 2006, **110**, 2821–2828.

[10] C. S. Cojocaru, A. Senger, and F. Le Normand, *J. Nanosci. Nanotechnol.*, 2006, **6**, 1331–1338.

[11] R. W. D. J. Warnatz, U. Maas, *Combustion*, Springer-Verlag, Berlin Heideberg New York, 2001.

[12] A. Lamprecht, B. Atakan, and K. Kohse-Hoinghaus, *Combust. Flame*, 2000, **122**, 483–491.

[13] J. Buldyreva, J. Bonamy, M. Weikl, F. Beyrau, T. Seeger, A. Leipertz, F. Vestin, M. Afzelius, J. Bood, and P.-E. Bengtsson, *J. Raman Spectrosc.*, 2006, **37**, 647–654.

[14] K. Bond, N. D. Collett, E. P. Fuller, J. L. Hardwick, E. E. Hinds, T. W. Keiber, I. S. G. Kelly-Morgan, C. M. Matthys, M. J. Pilkenton, K. W. Sinclair, and A. A. Taylor, *App. Physics B*, 2007, **90**, 255–262.

[15] A. S. Pine, *J. Quant. Spectrosc. Radiat. Transfer*, 1993, **50**, 149–166.

[16] H. Valipour and D. Zimmermann, *J. Chem. Phys.*, 2001, **114**, 3535–3545.

[17] S. W. Arteaga, C. M. Bejger, J. L. Gerecke, J. L. Hardwick, Z. T. Martin, J. Mayo, E. A. McIlhattan, J.-M. F. Moreau, M. J. Pilkenton, M. J. Polston, B. T. Robertson, and E. N.

Wolf, *J. Mol. Spectrosc.*, 2007, **243**, 253–266.

[18] J. P. Bouanich, D. Lambot, G. Blanquet, and J. Walrand, *J. Mol. Spectrosc.*, 1990, **140**, 195–213.

[19] J. P. Bouanich, G. Blanquet, and J. Walrand, *J. Mol. Spectrosc.*, 1999, **194**, 269–277.

[20] J. P. Bouanich, G. Blanquet, J. C. Populaire, and J. Walrand, *J. Mol. Spectrosc.*, 1998, **190**, 7–14.

[21] D. Lambot, G. Blanquet, J. Walrand, and J. P. Bouanich, *J. Mol. Spectrosc.*, 1991, **4150**, 164–172.

[22] J. P. Bouanich, J. Walrand, and G. Blanquet, *J. Mol. Spectrosc.*, 2002, **216**, 266–270.

[23] D. Lambot, J. C. Populaire, J. Walrand, G. Blanquet, and J. P. Bouanich, *J. Mol. Spectrosc.*, 1994, **165**, 1–11.

[24] D. Robert and J. Bonamy, *J. Phys.*, 1979, **40**, 923–943.

[25] S. Green, *Chem. Phys. Letters*, 1977, **47**, 119–122.

[26] L. Gomez, R. Z. Martínez, D. Bermejo, F. Thibault, P. Joubert, B. Bussery-Honvault, and J. Bonamy, *J. Chem. Phys.*, 2007, **126**, 204302–1–8.

[27] S. Green, *J. Chem. Phys.*, 1993, **98**, 257–268.

[28] S. Green and W. M. Huo, *J. Chem. Phys.*, 1996, **104**, 7590–7598.

[29] M. Mengel, D. C. Flatin, and F. C. De Lucia, *J. Chem. Phys.*, 2000, **112**, 4069–4075.

[30] X. Bruet, J. Bonamy, and M. L. Dubernet-Tuckey, *Chem. Phys.*, 2000, **254**, 297–307.

[31] J. M. Hutson, *Ann. Rev. Phys. Chem.*, 1990, **41**, 123–154.

[32] J. A. Pople, M. J. Frisch, and J. E. Del Bene, *Chem. Phys. Letters*, 1982, **91**, 185–189.

[33] M. J. Frisch, J. A. Pople, and J. E. Del Bene, *J. Chem. Phys.*, 1983, **78**, 4063–4065.

[34] A. M. Sapse and D. C. Jain, *J. Phys. Chem.*, 1984, **88**, 4970–4973.

[35] S. Topiol, A. M. Sapse, and J. Bunce, *Chem. Phys. Letters*, 1986, **124**, 514–516.

[36] C. E. Dykstra, *J. Am. Chem. Soc.*, 1990, **112**, 7540–7545.

[37] M. Yang and R. Watts, *J. Chem. Phys.*, 1994, **100**, 3582–3593.

[38] A.-M. Sapse, C. Pinto, and D. Jain, *J. Cluster. Science*, 2000, **11**, 327–332.

[39] B. Jeziorski, R. Moszynski, and K. Szalewicz, *Chem. Rev.*, 1994, **94**, 1887–1930.

[40] A. van der Avoird, P. E. S. Wormer, and R. Moszynski, *Chem. Rev.*, 1994, **94**, 1931–1974.

[41] G. Chalasinski and M. M. Szczesniak, *Chem. Rev.*, 1994, **94**, 1723–1765.

[42] A. J. Misquitta, R. Podeszwa, B. Jeziorski, and K. Szalewicz, *J. Chem. Phys.*, 2005, **123**,

214103–1–14.

[43] S. B. Boys and F. Bernardi, *Mol. Phys.*, 1970, **19**, 553–566.

[44] J. Santos, P. Cancio, J. L. Domenech, J. Rodriguez, and D. Bermejo, *Laser Chem.*, 1992, **12**, 53–63.

[45] Molpro is a package of ab initio programs written by H.-J. Werner and P. J. Knowles, with contributions from R. D. Amos, A. Berning, D. L. Cooper, M. J. O. Deegan, A. J. Dobbyn, F. Eckert, C. Hampel, G. Hetzer, T. Leininger, R. Lindh, A. W. Lloyd, W. Meyer, M. E. Mura, A. Nicklaß, P. Palmieri, K. Peterson, R. Pitzer, P. Pulay, G. Rauhut, M. Schütz, H. Stoll, A. J. Stone and T. Thorsteinsson.

[46] A. J. Sadlej, *Theor. Chim. Acta.*, 1991, **79**, 123–140.

[47] F. M. Tao and Y. K. Pan, *J. Chem. Phys.*, 1992, **97**, 4989–4995.

[48] V. Aquilanti, M. Bartolomei, D. Cappelletti, E. Carmona-Novillo, and F. Pirani, *J. Chem. Phys.*, 2002, **117**, 615–627.

[49] F. B. van Duijneveldt, J. G. C. M. van Duijneveldt-van de Rijdt, and J. H. van Lenthe, *Chem. Rev.*, 1994, **94**, 1873–1885.

[50] S. Green, *J. Chem. Phys.*, 1975, **62**, 2271–2277.

[51] A. van der Avoird, P. E. S. Wormer, and A. P. J. Jansen, *J. Chem. Phys.*, 1986, **84**, 1629–1635.

[52] W. H. Press, *Numerical Recipes in Fortran 77*, Cambridge University Press, 1992.

[53] J. M. Hutson and S. Green, *MOLSCAT version 14, Collaborative Computational Project 6 of the UK Science and Engineering Research Council*, Daresbury Laboratory, UK, 1995.

[54] A. Ben-Reuven, *Phys. Rev.*, 1966, **141**, 34.

[55] A. Ben-Reuven, *Phys. Rev.*, 1966, **145**, 7.

[56] R. Shafer and R. G. Gordon, *J. Chem. Phys.*, 1973, **58**, 5422–5443.

[57] D. Flower, *Cambridge Astrophysics Series vol. 17, Molecular collisions in the interstellar medium*, Cambridge University Press, Cambridge, 1990.

[58] A. E. DePristo and H. Rabitz, *J. Quant. Spectrosc. Radiat. Transfer*, 1979, **22**, 65–79.

[59] F. Thibault, B. Calil, J. Boissoles, and J.-M. Launay, *Phys. Chem. Chem. Phys.*, 2000, **2**, 5404–5410.

[60] F. Thibault, B. Calil, J. Buldyreva, M. Chrysos, J. M. Hartmann, and J. P. Bouanich, *Phys. Chem. Chem. Phys.*, 2001, **3**, 3924–3933.

[61] L. Gomez, B. Bussery-Honvault, T. Cauchy, M. Bartolomei, D. Cappelletti, and F. Pirani,

Chem. Phys. Letters, 2007, **445**, 99–107.

[62] J. M. Junquera-Hernández, J. Sánchez-Marín, and D. Maynau, *Chem. Phys. Letters*, 2002, **359**, 343–348.

[63] A. J. Russell and M. A. Spackman, *Mol. Phys.*, 1996, **88**, 1109–1136.

[64] R. Moszynski, P. E. S. Wormer, and A. van der Avoird, *J. Chem. Phys.*, 1995, **102**, 8385–8397.

[65] L. Gomez, R. Z. Martínez, D. Bermejo, and F. Thibault, *J. Quant. Spectrosc. Radiat. Transfer*, 2008, p. submitted.

[66] F. Thibault, R. Z. Martínez, J. L. Domenech, D. Bermejo, and J.-P. Bouanich, *J. Chem. Phys.*, 2002, **117**, 2523–2531.

[67] R. T. Pack, *J. Chem. Phys.*, 1978, **70**, 3424–3433.

[68] W. B. Neilsen and R. G. Gordon, *J. Chem. Phys.*, 1973, **58**, 4131–4148.

[69] W. B. Neilsen and R. G. Gordon, *J. Chem. Phys.*, 1973, **58**, 4149–4170.

FIG. 1: Selected angular cuts of the PES as a function of the intermolecular distance R. Symbols represent the *ab initio* values. CCSD(T) *ab initio* energies are compared with SAPT(DFT) values for three angular approaches.

FIG. 2: Main anisotropic components of the PES (see eq. (1)).

FIG. 3: Selected partial pressure broadening cross section $\sigma\left(j_A, j_B; E_{kin}\right)$ [in Å^2] as a function of the relative kinetic energy [in cm^{-1}].

FIG. 4: Comparison between experimental and calculated PB coefficients of isotropic Raman lines. Displayed theoretical values are the ones obtained through the thermal average of the PB cross section and the ones at the single kinetic energy $\frac{4}{\pi}k_BT/hc$ associated to the mean speed at 143 K.

FIG. 5: Comparison between experimental[6, 22] pressure broadening coefficients of R lines and calculated (same as Fig. 4) values for Q lines at 173 K.

FIG. 6: Comparison between experimental[6, 21] pressure broadening coefficients of R lines and calculated (same as Fig. 4) values for Q lines at 295 K.